Hadas Ziso[1]
Robotics Laboratory,
Department of Mechanical Engineering,
Technion,
Haifa 32000, Israel
e-mail: hadasz@tx.technion.ac.il

Moshe Shoham
Fellow ASME
Tamara and Harry Handelsman Academic Chair
US National Academy of Engineering
Foreign Member, Robotics Laboratory Director,
Department of Mechanical Engineering,
Technion,
Haifa 32000, Israel
e-mail: shoham@technion.ac.il

Bending Instability of a General Cross Section Thin-Wall Tube for Minimal Radius of Curvature Passage

This paper describes an analytical tool for the design of thin-wall tubes for passage through minimal radius of curvature trajectory. The design is based on a model of thin-wall tube buckling under pure bending. An extended analytical solution for general initial cross section is found based on Brazier method by energy theory of elastic stability. The model predicts the critical moment, curvature, flattening, and stress and allows choosing the most suitable cross section shape for a specific purpose. For example, tubes with ocular and rounded-ocular cross sections were found suitable for semiflexible applications such as endoscopy, where they elastically cross a sharp corner. [DOI: 10.1115/1.4028220]

1 Introduction

The motivation for this paper comes from the field of endoscopy. It is often necessary for an endoscope to cross a steep corner in order to reach a designated target. The common endoscopic devices have a fixed joint or "knee" at its edge that enables a constant predefined length of the remaining tool distal to the corner (Fig. 1). In the design suggested here, the joint is "floating" as the tube progresses through the corner, resulting in a tunable postcorner straightened tube. In addition, the endoscopic devices are usually limited to relatively large bending radius, preventing passage through narrow curved places. The tube cannot be too flexible, as it has to maintain some rigidity upon exit from the corner. The nonlinear mechanism we present here allows minimizing the bending radius of the endoscopic end knee without crossing the elastic region, on the one hand, while being rigid enough to sustain lateral load at the straighten part on the other hand. The most suitable cross section tube shape is found according to the desired specifications of corner curvature and load bearing, with circumferential stress minimization for elastic behavior. This mechanism is modeled hereby as pure moment acting on an infinitely long thin-wall tube.

Generally, there are several types of equilibrium paths in the buckling behavior of structures. In the case studied here, the primary equilibrium path of ovalization resembles a snap-through type (Fig. 2). A secondary equilibrium path of buckling under axial load, which we do not analyze here, may occur at the compression side if the compressive stress reaches the critical bifurcation stress (analytically approximated by $\sigma_{\text{cr\_b}} = (1/\sqrt{3(1-\nu^2)})$ $(Et/r) \cong (0.6Et/r)$ for $\nu = 0.3$ [1]). In such case, there is a bifurcation point between the two paths, and the secondary equilibrium path is followed [2,3]. The primary equilibrium path of thin-wall tube structural buckling as a result of a pure bending moment involves a change in the tube's cross section shape. As the curvature increases, the shape is flattened or ovalized during a nonlinear, buckling event. This event is characterized in a progressive reduction in the shell's bending rigidity. Eventually, a maximum value of the moment is reached; further bending occurs at a dropping moment and stress (Fig. 2).

The instability phenomenon for such tubes due to ovalization of their cross sections induced by bending was first investigated by Brazier [4] in 1927. He showed analytically that when an initial infinite straight tube with a circular cross section is bent uniformly, the longitudinal tension and compression that resist the applied bending moment also tend to flatten or ovalize the cross section of the tube. Brazier found that under steadily increasing curvature the bending moment, being the product of curvature and flexural stiffness, has a maximum value that is thus defined as the instability critical moment.

Following Brazier's original study, a great deal of work relating to bending stability analysis of circular cross section tubes has been done [1,5–11], confirming his results. Brazier analysis predicts quite well the moment up to its maximal critical value; however, it does not predict the postbuckling behavior. Modifications to improve Brazier's postbuckling analysis were investigated by Karamanos [1], however with values ∼20% higher than Brazier's.

Most of the studies investigating thin-wall tube buckling were done on circular cross sections. As for oval or general cross section tubes, a few studies were done on buckling under axial load [12–15], and even fewer considering pure bending [2,3,16]. Except for Firer and Sheinman [12] who investigated general cross section shapes, the analysis was confined to either elliptic, oval, or square cross sections. None of those studies solved the equations analytically.

In the present study, we have developed an analytical tool for the design of thin-wall tubes for buckling applications needed, for example, to cross a sharp corner and maintain its elastic properties at the exit side. This tool allows choosing the most suitable cross section shape for a special purpose design. The analysis is based on Brazier's and Karamanos's instability model of thin-wall tubes and solved by energy theory of elastic stability. First, we added an extended Fourier series to Brazier's assumption of flattening shape due to bending to further generalization, previously done numerically only [17]. These added terms to the circumferential bending strain energy, the longitudinal bending strain energy and the resulting solution. Second, we broaden the method for initially general cross section shape, represented by either a simple radius–angle relations or in the most general case by a truncated Fourier series. The energy method applied to Brazier method by Calladine [7], Li [9], and others is used here as well.

1.1 Analytical Model Based on Energy Theory of Elastic Stability. The instability of tubes under pure bending is analyzed here using the energy theory of elastic stability. The critical load of a structure is the load at which the structure loses its stability, or changes from stable to unstable equilibrium position. In terms
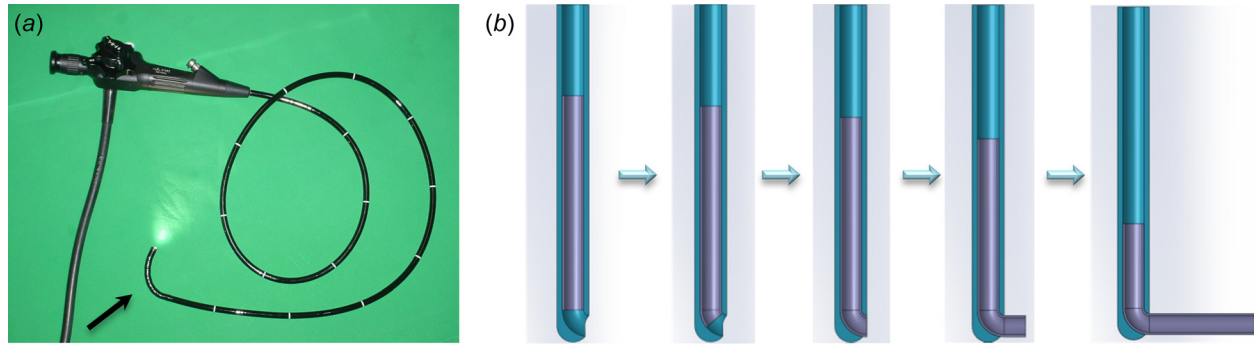
Fig. 1 (*a*) A common endoscope with a fixed, low curvature joint (arrow). (*b*) Our mechanism as a part of an endoscopic device with high curvature, "floating" joint.

of potential energy, its second variation will no longer be positive definite [18]. The total strain energy of a thin-wall tube under pure bending is comprised of the circumferential bending strain energy (flattening or ovalization related) and the longitudinal bending strain energy, and is thus given by

$$\Pi = U_\theta + U_L + U_M \tag{1}$$

where U_θ is the circumferential bending strain energy, U_L is the longitudinal bending strain energy, and $U_M = -MCL$ is the potential energy of the applied moment. The condition in which the potential energy ceases to be positive definite is found based on the Lagrange–Dirichlet theorem [19] by

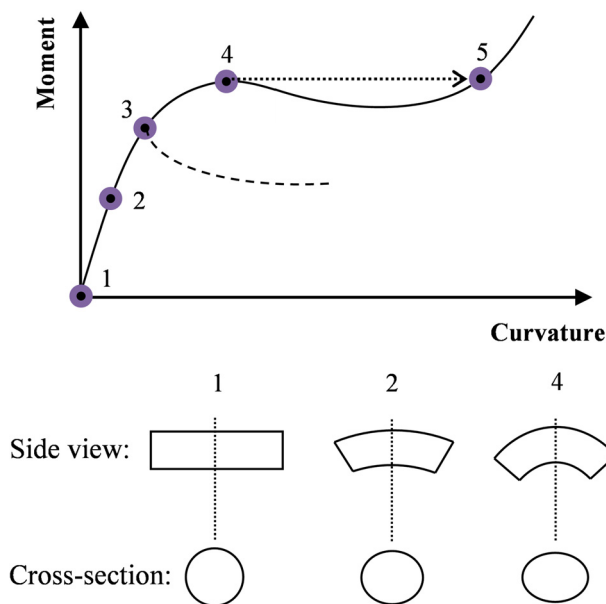$$\frac{d\Pi}{dq_i} = 0 \tag{2}$$

Fig. 2 The process of thin-wall tube buckling as a result of pure bending moment. The solid line represents the primary equilibrium path; the dashed line—secondary equilibrium path. Point 1: initial state with no external moment; point 2: beginning of ovalization as a result of pure moment; point 3: bifurcation point, in which the secondary equilibrium path will be followed if buckling as a result of compression occurs; point 4: ovalization critical point, where the tube becomes unstable and snaps to point 5 (dashed arrow).

$$\begin{vmatrix} \dfrac{\partial^2 \Pi}{\partial q_i^2} & \dfrac{\partial^2 \Pi}{\partial q_i \partial q_j} & \dfrac{\partial^2 \Pi}{\partial q_i \partial q_k} \\[2ex] \dfrac{\partial^2 \Pi}{\partial q_j \partial q_i} & \dfrac{\partial^2 \Pi}{\partial q_j^2} & \dfrac{\partial^2 \Pi}{\partial q_j \partial q_k} & \cdots \\[2ex] \dfrac{\partial^2 \Pi}{\partial q_k \partial q_i} & \dfrac{\partial^2 \Pi}{\partial q_k \partial q_j} & \dfrac{\partial^2 \Pi}{\partial q_k^2} \\[2ex] & \vdots & \end{vmatrix} = 0 \tag{3}$$

were the parameters q_i can be, for example, the longitudinal bending curvature of the tube C and flattening of the extreme fibers ξ ($q_1 = C, q_2 = \xi$). For finding the applied moment M as a function of curvature C, only Eq. (2) is solved.

1.2 Brazier Method. When a long, originally straight, thin-wall tube with circular cross section is subjected to pure bending moment, the tensile and compressive longitudinal stresses on opposite sides of the natural plane combined with the curvature along the tube axis flatten the cross section into an oval shape. Thus, the deformations of the tube can be characterized by the longitudinal bending deformation (longitudinal bending curvature) and the cross section bending deformation (ovalization). To formulate these deformations, the following assumptions are made [4]:

(1) The ovalization is uniform along the length of the infinite tube and can be approximated as

$$w = \xi a_0 \cos(2\theta) \tag{4}$$

where w is the radial component of displacements, a_0 is radius of a circular cross section tube; θ is the angular coordinate measured from neutral plane in the original configuration, and ξ is the dimensionless parameter characterizing the maximum flattening at the extreme fibers (Fig. 3). ξ is an unknown coefficient, and is represented in Eq. (4) as a coefficient of a truncated Fourier series. Note that the change of location along y as a result of beam bending is not analyzed here (adds a nonsymmetric term to the displacement [10]).

(2) The cross section deforms inextensionally in its own plane [7], and is approximated by

$$\varepsilon_\theta = \frac{1}{a_0}\left(\frac{dv}{d\theta} + w\right) = 0 \tag{5}$$

where ε_θ is the circumferential extension strain and v is the circumferential component of displacements. Note that (w/a_0) represents the radial expansion and $(dv/a_0 d\theta)$ represents the relocation.
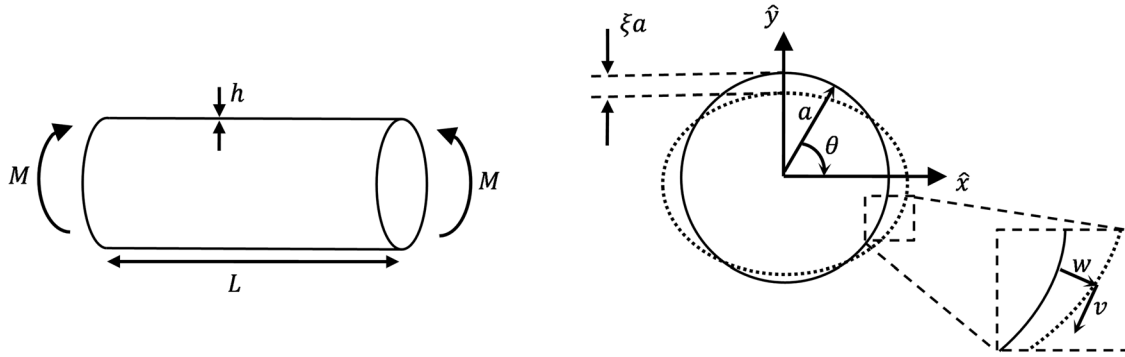
Fig. 3 Longitudinal bending of initially straight tube under pure moment and the resulted cross-sectional deformation (dashed line). w and v are the radial and circumferential components of displacement, correspondingly, as shown in the enlarged box.

Brazier found the following circumferential bending strain energy and the longitudinal bending strain energy:

$$U_\theta = \frac{3\pi LE}{8a_0} \frac{h^3}{1-\nu^2} \xi^2 \qquad (6)$$

$$U_L = \frac{\pi L}{2} Eha_0^3 \left(1 - \frac{3}{2}\xi\right) C^2 \qquad (7)$$

1.3 Modified Brazier Method. Karamanos modified Brazier method by generalizing the second moment of area of the tube cross section in the deformed configuration, resulting in the following longitudinal bending strain energy [1]:

$$U_L = \frac{\pi L}{2} Eha_0^3 \left(1 - \frac{3}{2}\xi + \left[\frac{5}{8}\xi^2\right]\right) C^2 \qquad (8)$$

where the term in the square brackets is the addition to Brazier solution.

Karamanos method predicts quite well the ovalization extent ξ as a function of the curvature, when compared to 2D Finite Elements results. It also enables prediction of the postbuckling behavior of the moment as a function of the curvature; however, it has values higher in ~20% than Brazier's.

2 Methods

2.1 Extended Brazier Method for Circular Cross Section. In our study, the radial component of displacements in Eq. (4) is further generalized by extending it with a Fourier series into [17]

$$w = a_0(\xi_1 \cos(2\theta) + \xi_2 \cos(4\theta) + \cdots + \xi_n \cos(2n\theta)) \qquad (9)$$

where the flattening is given by w at $\theta = \pi/2$. Note that the ovalization is symmetric in relation to x and y axes. The energy equations (Eqs. (2) and (3)) in this case includes more parameters: $q_1 = C, q_2 = \xi_1, q_3 = \xi_2, \ldots, q_{n+1} = \xi_n$. For simplicity, the following equations were calculated with a truncated Fourier series at $n = 2$. The circumferential curvature change of a circular cross section is approximated by [19]

$$\chi_\theta = \frac{1}{a_0^2} \left(\frac{dv}{d\theta} - \frac{d^2w}{d\theta^2}\right) \qquad (10)$$

The circumferential moment is given by

$$M_\theta = D\chi_\theta \qquad (11)$$

where D is the bending stiffness, defined as $D \equiv (Eh^3/12(1-\nu^2))$. The circumferential bending strain energy for circular cross section

can be expressed as follows by using Eqs. (5), (10), and (11), taking into account $M_{x\theta} = M_x = 0$:

$$U_\theta = \frac{L}{2}\int_0^{2\pi} M_\theta \chi_\theta a_0 d\theta = \frac{L}{2}\frac{Eh^3}{12(1-\nu^2)}\int_0^{2\pi}\left[\frac{1}{a_0^2}\left(w + \frac{d^2w}{d\theta^2}\right)\right]^2 a_0 d\theta \qquad (12)$$

where L is the tube's length, h is the wall thickness, E is the elastic modulus of the tube in the circumferential direction, and ν is Poisson's ratio. Equation (9) is substituted into Eq. (12), yielding for an initial circular cross section

$$U_\theta = \frac{3\pi LE}{8a_0} \frac{h^3}{1-\nu^2} \left(\xi_1^2 + 25\xi_2^2\right) \qquad (13)$$

The longitudinal bending strain energy is calculated by considering the pure bending of the tube having a given deformed cross section, which is

$$U_L = \frac{L}{2} EI(\xi) C^2 \qquad (14)$$

where $I(\xi)$ is the second moment of area of the tube cross section in the deformed configuration, which can be calculated for circular cross section by

$$I(\xi) = h \int_0^{2\pi} y^2 a_0 d\theta \qquad (15)$$

Given $y = (w + a)\sin\theta + v\cos\theta$ (from geometry), calculating the moment of inertia using Eqs. (5), (9), and (15) and substituting it into Eq. (14), the longitudinal energy for an initial circular cross section becomes

$$U_L = \frac{\pi L}{2} Eha_0^3 \left(1 - \frac{3}{2}\xi_1 + c_2\xi_2 + \left[\frac{5}{8}\xi_1^2 - \frac{5}{16}\xi_1\xi_2 + \frac{17}{32}\xi_2^2\right]\right) C^2 \qquad (16)$$

For circular cross section shape the coefficient c_2 equals zero, however, this is not the case for other cross section shapes. The solution using Eq. (16) is referred to here as Modified & Extended Brazier method. Similar to Brazier, we neglected the term in the square brackets, resulting in

$$U_L = \frac{\pi L}{2} Eha_0^3 \left(1 - \frac{3}{2}\xi_1 + c_2\xi_2\right) C^2 \qquad (17)$$

The solution using Eq. (17) is referred to here as Extended Brazier method.
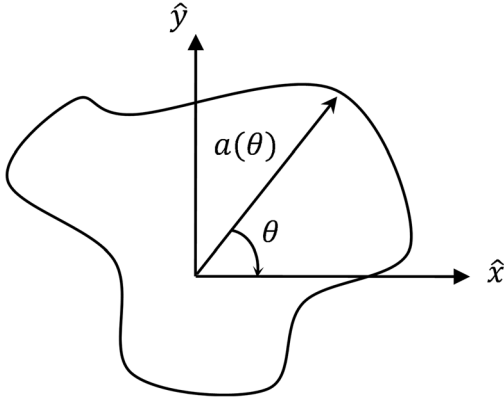
Fig. 4 The general cross section shape, represented by $a(\theta)$

Substituting Eqs. (13) and (16) (or Eq. (17)) into Eqs. (1), (2), and (3), the critical moment, the critical bending curvature, and the critical ovalization terms $\xi_{1_{cr}}, \xi_{2_{cr}}$ can be obtained:

$$M_{cr} = M_0 \frac{Ea_0 h^2}{\sqrt{1 - \nu^2}} \tag{18}$$

$$C_{cr} = C_0 \frac{h}{a_0^2 \sqrt{1 - \nu^2}} \tag{19}$$

The maximal critical circumferential stress is given by

$$\sigma_{cr} = \frac{M_{cr} y_{max}}{I(\xi)} \equiv \sigma_0 \frac{Eh}{a_0 \sqrt{1 - \nu^2}} \tag{20}$$

where y_{max} is the most extreme location after the deformation in y direction. $M_0, C_0,$ and σ_0 are normalized values of the moment, curvature, and stress, respectively.

2.2 Generalized Solution Cross Section Shape. A few modifications to Brazier method are made in order to analyze the bending stability for general cross section shape. The general cross section shape radius depends on the angle and denoted as $a = a(\theta)$ (Fig. 4). Equation (5) is also valid for general cross section shape, replacing the constant radius a_0 with $a(\theta)$ [20]. Equation (10) for general cross section shape becomes

$$\chi_\theta = \frac{1}{a} \frac{d}{d\theta} \left(\frac{v}{a} - \frac{1}{a} \frac{dw}{d\theta} \right) \tag{21}$$

The line integral of a function along the shape's path C in polar coordinates is given by

$$\int_C f(x,y) ds = \int_a^b f(a(\theta)) \sqrt{a^2 + (da/d\theta)^2} d\theta$$

where

$$ds = \sqrt{a^2 + (da/d\theta)^2} \cdot d\theta$$

Equation (12) thus becomes

$$U_\theta = \frac{L}{2} \int_0^{2\pi} M_\theta \chi_\theta \sqrt{a^2 + \left(\frac{da}{d\theta}\right)^2} d\theta \tag{22}$$

and Eq. (15) becomes

$$I(\xi) = h \int_0^{2\pi} y^2 \sqrt{a^2 + \left(\frac{da}{d\theta}\right)^2} d\theta \tag{23}$$

For example, Eq. (22) for elliptic cross section shape according to Brazier method (compared to Eq. (6)) is

$$U_\theta = 1.1849 \cdot \frac{3\pi L E}{8a_0} \frac{h^3}{1 - \nu^2} \xi^2 \tag{24}$$

Note that the integrals by θ were calculated numerically due to the complicated terms in the integrand.

2.2.1 Initial Cross Section Shape Representation. We have investigated several special shapes in addition to the general cross section shape, including an ellipse, an oval shape, an ocular shape, and a rounded-ocular shape. In order to compare between the different shapes, represented by $a(\theta)$, their perimeter was normalized by $2\pi a_0$, that is the perimeter of a circle with a radius a_0. The perimeter normalization factor R_p, was obtained by $R_p = \left(\int_0^{2\pi} \sqrt{a(\theta)^2 + (da(\theta)/d\theta)^2} d\theta \right) / 2\pi a_0$. Other shape normalization options are demonstrated in Sec. 3.3.

The curvature $(1/a(\theta))$ of a general cross section shape, such as a rounded-ocular shape, is fitted by a truncated Fourier series in the form of [12]

$$a(\theta) = \frac{a_0}{R_p} \frac{1}{\sum\limits_{n=0}^{N} b_n \cos(2n\theta)} \tag{25}$$

The ellipse shape is represented by

$$a(\theta) = \frac{a_0}{R_p} \frac{b \cdot k}{\sqrt{b^2 \cdot \cos^2(\theta) + k^2 \cdot \sin^2(\theta)}} \tag{26}$$

where k and b are the major and minor semi-axes, $f = \pm \sqrt{(k^2 - b^2)}$ is the focus location and $e = f/k$ is the eccentricity.

The oval shape is represented by

$$a(\theta) = \frac{a_0}{R_p} \frac{1}{1 - q\cos(2\theta)} \tag{27}$$

where q is the eccentricity coefficient. Note that the oval shape eccentricity (q) in Eq. (27) resembles $\sim 1/3$ of the ellipse eccentricity (e).

An ocular cross section shape, composed of two opposite arcs, was also investigated. Each of the ocular shape's arcs is represented by

$$a(\theta) = \frac{a_0}{R_p} \left(\pm b_0 \sin(\theta) + \sqrt{R_0^2 + b_0^2 \sin^2(\theta) - b_0^2} \right) \tag{28}$$

where R_0 is the arc's radius and b_0 is the arc center shift in y direction.

3 Results

In this section, the analysis results are presented in two ways: first, the different solution methods for a circular cross section are compared; second, analysis of different cross section shapes is performed by Extended Brazier method for choosing the most suitable cross section shape for a specific purpose.

3.1 Comparison of Different Solution Methods for Circular Cross Section. The solution for the critical moment and curvature of a tube with circular cross section was analytically found in five different methods: Brazier method; Modified Brazier method, as in Eq. (8); Extended Brazier method, as in Eq. (9); Modified & Extended Brazier method, as in Eq. (16); and Calladine method [7]. The bending moment caused the expected ovalization effect acting on a circular cross section tube, as discussed above. The critical ovalization factor caused by the bending moment according to Brazier method [4], namely ξ_{cr}, equals $(2/9) \cong 0.22$ and occurs at the relative maximum of the bending moment as a function of the curvature. The critical moment factor in this method, namely
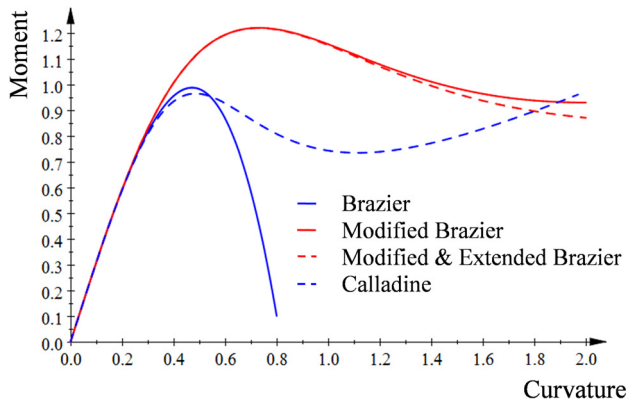
Fig. 5 The moment as a function of curvature (normalized) of an initially circular cross section shape solved in four different methods

Table 1 Percent of reduction in critical moment factor, critical stress factor and critical curvature factor solved by Extended Brazier method compared to Brazier method for oval, elliptic, ocular, and rounded-ocular cross section shapes

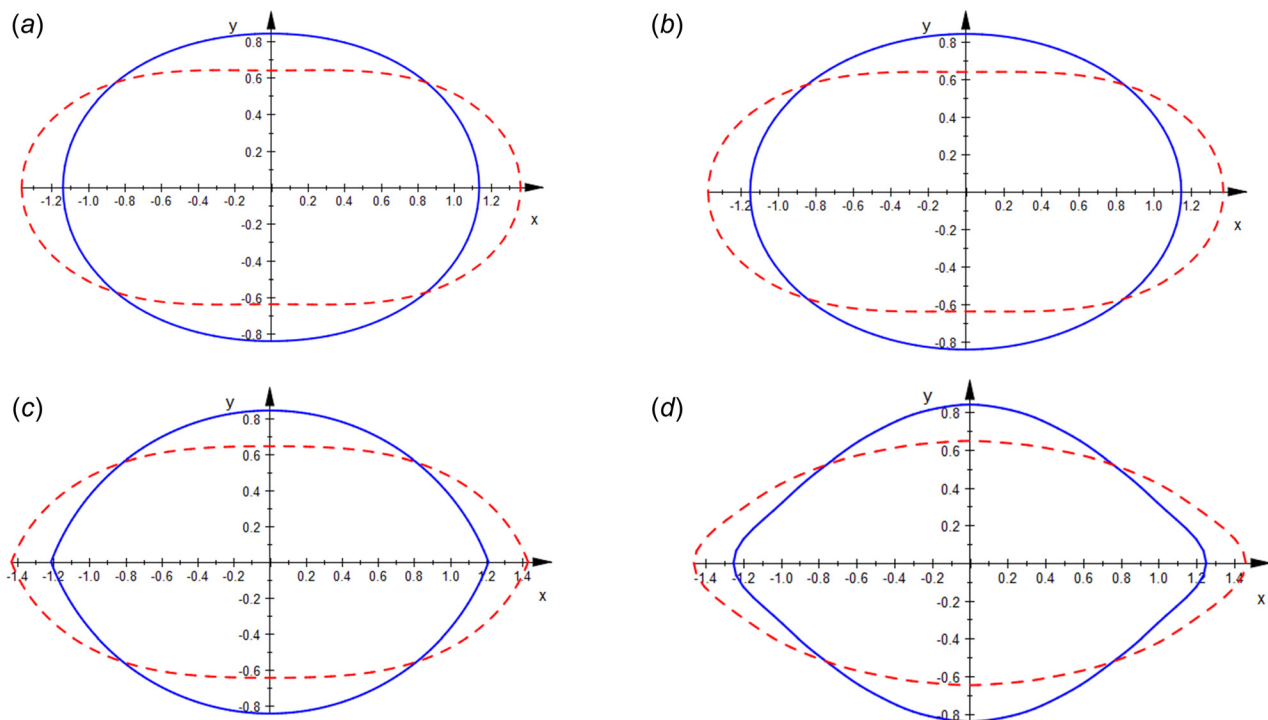|	Oval	Elliptic	Ocular	Rounded-ocular
σ_0 (%)	3.8	3.0	1.7	6.6
M_0 (%)	4.0	3.4	3.1	7.9
C_0 (%)	4.0	3.4	3.1	7.9

M_0, equals $\left[(\pi 2\sqrt{2})/9\right] \cong 0.987$, the critical curvature factor is $C_0 = \left(\sqrt{2}/3\right) \cong 0.471$ and the critical stress factor, taking into account the shape change when calculating the moment of inertia (Eq. (20)), is $\sigma_0 = \left((7\sqrt{2})/27\right) \cong 0.367$. Brazier originally calculated it using the initial moment of inertia of a circle and $y_{\max} = a_0$, resulting in $\sigma_0 \cong 0.314$.

The results of the different methods are all very close to Brazier's solution nearly up to the critical curvature (Fig. 5). Calladine's solution is the closest to Brazier's solution in the prebuckling stage. It is also better than the other solutions as it describes the postbuckling behavior more accurately, as previously verified by others with finite element analysis [1]. The Modified Brazier method results in a legitimate moment–curvature trend; however, the critical moment is ∼20% higher than expected and occurs at much higher curvature. Note that Extended Brazier's solution is almost identical Brazier's solution for circular cross section shape, thus it is not shown in the graph. The results of the methods for other cross section shape have similar graphs (data not shown). The Extended Brazier method in noncircular shapes resulted in a slight change in the results (Table 1). All values in the Extended Brazier method were smaller than those in the Brazier method. Equation (17) was used for Extended Brazier method with two terms, ξ_1, ξ_2, as the effect of more terms was negligible; for example, the first three terms of an oval shape $(q = 0.15)$ are $\xi_1 = 0.219, \xi_2 = 5.83 \times 10^{-2}\xi_1, \xi_3 = 4.81 \times 10^{-3}\xi_1$.

3.2 Analysis Results of Different Cross Section Shapes in Extended Brazier Method. The solution for the critical moment and curvature of a tube with different cross section shapes was analytically found in four different methods: Brazier method; Modified Brazier method, as in Eq. (8); Extended Brazier method, as in Eq. (9); and Modified & Extended Brazier method, as in Eq. (16). For brevity, only the results of Extended Brazier method are presented hereby. The ovalization effect on different cross section shapes was found analytically and demonstrated graphically (Fig. 6). All shapes have the same perimeter and the same maximal height (at y direction).

According to Extended Brazier solution, all shapes have lower critical moment and higher critical curvature than those of a circular cross section (Fig. 7). The oval and elliptic shapes resulted in very similar graphs, as expected. The ocular shape has lower moment than that of the oval or elliptic shape, and the rounded-

Fig. 6 Different initial cross section shapes (solid line) and the flattened shapes in the critical state (dashed line). (a) Oval shape, (b) elliptic shape, (c) ocular shape, and (d) rounded-ocular shape.
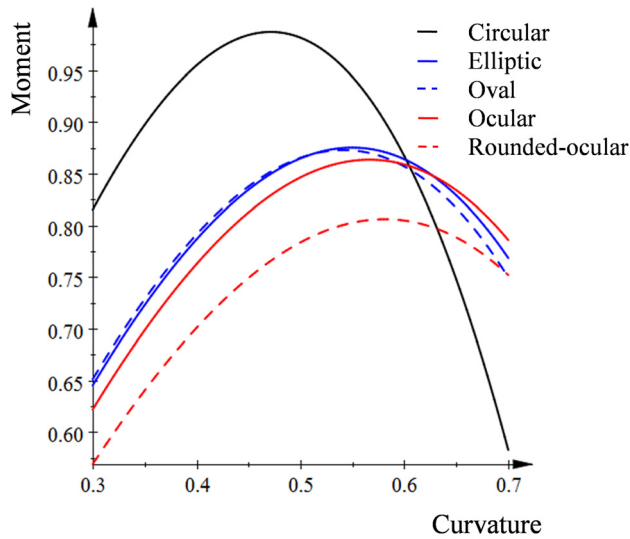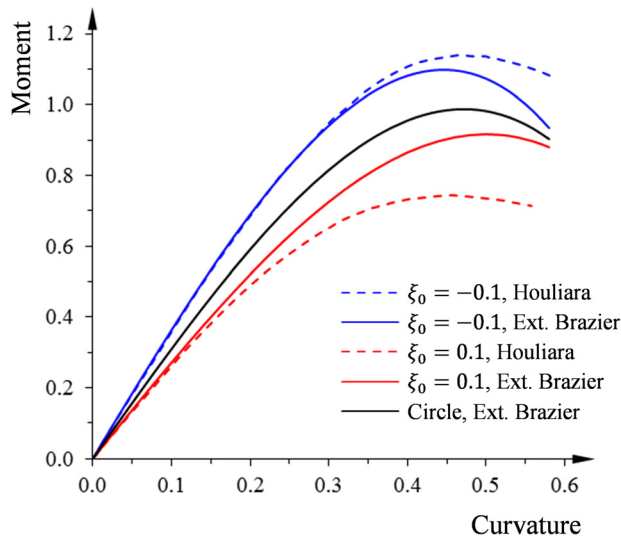
Fig. 7 The moment as a function of curvature (normalized) for different initial cross section shapes solved in Extended Brazier method

ocular shape resulted in the lowest critical moment and highest critical curvature.

The critical stress factor of each shape (σ_0 in Eq. (20)) was also calculated. The critical stress factor of the oval, elliptic, and ocular shapes was lower than that of a circular shape; however, the critical stress factor of the rounded-ocular shape was higher than that of the circular shape in 2.7%.

In addition, we compared our results to those of Houliara [21], analyzing a tube with initial ovalization in the form of Eq. (4), given by $a(\theta) = a_0(1 + \xi_0 \cos(2\theta))$. The results of Extended Brazier solution for $\xi_0 = 0.1$, $\xi_0 = 0$ (circle), and $\xi_0 = -0.1$ are displayed together with Houliara's and Karamanos [21] numerical results (Fig. 8). Our results for $\xi_0 = -0.1$ are in good agreement with the numeric results nearly up to the critical point. For $\xi_0 = 0.1$ our results are in good agreement with the numeric results for lower curvatures (up to ~ 0.2). It shows a similar trend of decreased critical moment, yet higher than the numeric.

Fig. 8 The moment as a function of curvature (normalized) for oval initial cross section shape solved in Extended Brazier method and numerically by Houliara

Table 2 The critical moment, stress, and curvature according to Extended Brazier method, found for shapes under the criteria of spec A: equal width of 3 (mm) and critical curvature of 5 (mm) with maximal deflection of 1 (mm) under lateral load of 0.75 (N mm). The analyzed cross section shapes are: circular ($a_0 = 1.5$ (mm)), elliptic (height 0.98 (mm)), ocular (height 1.07 (mm)), and rounded-ocular (height 1.03 (mm)).

	Circular	Elliptic	Ocular	Rounded-ocular
M_{cr} (MPa)	55	33	29	30
σ_{cr} (Mpa)	60	134	122	124
$1/C_{cr}$ (mm)	29.2	4.4	5	4.8
Deflection under load (mm)	0.1	1	1	1

3.3 Examples of Designs. A "semiflexible" tube for endoscopic application was designed as an example for utilizing the design tool developed here which further can be applied for minimally invasive surgeries. The "semiflexible" tube specification included ability to elastically reach high curvature, on the one hand; and remain sufficiently rigid under a desired level of lateral load after exiting the corner, on the other hand. The load F is defined here as a point force load acting at the edge of a fixed tube and the deflection is calculated at the edge by $(FL^3/3EI)$; in the following examples the tube length L was 30 (mm) and the load FL was 0.75 (N mm) and 7.5 (N mm). The critical stress of the tube must be below material yield stress in order for it to remain elastic. In addition, wall thickness to radius ratio should be higher than 0.1 in order to avoid wrinkles as a result of compression related buckling (bifurcation); in the following examples it was taken as 0.15 (mm). The critical moment, stress, and curvature of the different shaped tubes were calculated for an isotropic material with Young modulus of 1.5 GPa and Poisson ratio of 0.4.

Tube design by most suitable cross section shape selection is demonstrated for three different specifications, suitable for different applications: limited width for minimally invasive endoscopy (spec A); limited perimeter for material weight/price minimization (spec B); and limited height for higher load bearing capabilities (spec C).

3.3.1 Spec A. The spec for this design is: cross section shape width of 3 (mm); reach critical curvature of 5 (mm); and sustain lateral load of 0.75 (N mm) with maximal deflection of 1 (mm). The cross section shapes that were analyzed for spec A are: a circle with $a_0 = 1.5$ (mm); an ellipse bounded in 0.98×3 (mm^2); an ocular shape bounded in 1.07×3 (mm^2); and a rounded-ocular shape bounded in 1.03×3 (mm^2) (Table 2).

It was found that the circular shape with $a_0 = 1.5$ (mm) has the lowest deflection under the defined load; however, it is far from the desired critical curvature of 5 (mm). The elliptic shape reaches even higher curvature than the desired, yet with higher critical

Table 3 The critical moment, stress, and curvature, according to Extended Brazier method, found for shapes under the criteria of spec B: equal perimeter of 3π (mm) and critical curvature of 10 (mm) with maximal deflection of 0.4 (mm) under lateral load of 0.75 (N mm). The analyzed cross section shapes are: circular ($a_0 = 1.5$ (mm)), elliptic (bounded in 1.39×4.24 (mm^2)), ocular (bounded in 1.55×4.35 (mm^2)), and rounded-ocular (bounded in 1.48×4.3 (mm^2)).

	Circular	Elliptic	Ocular	Rounded-ocular
M_{cr} (MPa)	55	47	42	43
σ_{cr} (Mpa)	60	95	84	87
$1/C_{cr}$ (mm)	29.2	8.9	10.6	9.8
Deflection under load (mm)	0.1	0.36	0.33	0.36

Table 4 The critical moment, stress, and curvature according to Extended Brazier method, found for shapes under the criteria of spec C: equal height of 3 (mm) and critical curvature of 30 (mm) with maximal deflection of 1 (mm) under lateral load of 7.5 (N mm). The analyzed cross section shapes are: circular ($a_0 = 1.5$ (mm)), elliptic (bounded in 3×9.15 (mm²)), ocular (bounded in 3×8.42 (mm²)), and rounded-ocular (bounded in 3×8.73 (mm²)).

	Circular	Elliptic	Ocular	Rounded-ocular
M_{cr} (MPa)	55	102	82	87
σ_{cr} (Mpa)	60	44	43	43
$1/C_{cr}$ (mm)	29.2	41.4	39.6	40.4
Deflection under load (mm)	0.94	0.36	0.46	0.43

moment and stress. This could be problematic if the material yield stress is lower than this value. The ocular and the rounded-ocular shapes result in lower stress than the elliptic shape, and reach the desired critical curvature. These shapes are therefore the most suitable shapes for spec A.

3.3.2 Spec B. The spec for this design is: cross section shape perimeter of 3π (mm); reach critical curvature of 10 (mm); and sustain lateral load of 0.75 (N mm) with maximal deflection of 0.4 (mm). The cross section shapes that were analyzed for spec B are: a circle with $a_0 = 1.5$ (mm); an ellipse bounded in 1.39×4.24 (mm²); an ocular shape bounded in 1.55×4.35 (mm²); and a rounded-ocular shape bounded in 1.48×4.3 (mm²) (Table 3).

It was found that the circular shape with $a_0 = 1.5$ (mm) has the lowest critical stress; however, it does not reach the desired critical curvature of 10 (mm). The elliptic shape reaches even higher curvature than the desired, yet with higher critical stress. The ocular shape results in lower stress than the elliptic shape, however it did not reach the desired critical curvature. The rounded-ocular shape fulfilled all the requirements and is thus the most suitable shape for spec B.

3.3.3 Spec C. The spec for this design is: cross section shape height of 3 (mm); reach critical curvature of 30 (mm); and sustain lateral load of 7.5 (N mm) with maximal deflection of 1 (mm). The cross section shapes that were analyzed for spec C are: a circle with $a_0 = 1.5$ (mm); an ellipse bounded in 3×9.15 (mm²); an ocular shape bounded in 3×8.42 (mm²); and a rounded-ocular shape bounded in 3×8.73 (mm²) (Table 4).

It was found that the elliptic, ocular and rounded-ocular have the lowest critical stress; however, it does not reach the desired critical curvature of 30 (mm). The circular shape with $a_0 = 1.5$ (mm) is the only shape that reaches the desired critical curvature of 30 (mm) and sustain the desired level of lateral load; It is, thus, the most suitable shape for spec C.

4 Discussion and Conclusions

In this paper we have implemented the energy method to Brazier method for general cross section shapes and further extended the solution to include more general flattening. We have represented the general cross section shape in the most general form by a truncated Fourier series, and also investigated some shapes of interest.

It was found that Brazier assumption of oval flattening shape is only valid for initial circular cross section shape; for other shapes the Extended Brazier method's truncated Fourier series have more than one significant term. In these cases, the Extended Brazier method resulted in reduced stress, moment and curvature relating to Brazier method.

Brazier found an analytical solution for circular cross sections only, valid up to the critical point. Modified Brazier method, as suggested by Karamanos, predicts the postbuckling trend of moment versus curvature quite well, however with values ∼20%

higher than Brazier's. Calladine method is the most suitable for that purpose for circular cross sections; however it is not straight forward extendable to general cross sections.

The method described in this paper provides a novel, simple, and intuitive tool for the selection of the most suitable cross section tube's shape for a specific application. It was found that different cross section shapes are suitable for different specifications, as previously defined: the ocular and rounded-ocular shapes are the most suitable for Spec A, representing limited width applications under low loads and high curvature, such as minimally invasive endoscopy; the rounded-ocular shape is the most suitable for Spec B, representing limited perimeter applications, when material weight/price should be minimized, under low loads and moderate curvature; and the circular shape is the most suitable for Spec C, representing limited height applications under high loads and low curvature. When designing a tube for applications such as a semiflexible endoscopy, it is therefore recommended to consider noncircular cross section shapes.

References

[1] Karamanos, S. A., 2002, "Bending Instabilities of Elastic Tubes," Int. J. Solids Struct., **39**(8), pp. 2059–2085.
[2] Kempner, J., and Chen, Y. N., 1974, "Buckling and Initial Postbuckling of Oval Cylindrical Shells Under Combined Axial Compression and Bending," Trans. N. Y. Acad., Sci., **36**(II), pp. 171–191.
[3] Vaziri, A., 2009, "Mechanics of Highly Deformed Elastic Shells," Thin-Walled Struct., **47**(6-7), pp. 692–700.
[4] Brazier, L. G., 1927, "On the Flexure of Thin Cylindrical Shells and Other 'Thin Sections," Proc. R. S. London A, **116**(773), pp. 104–114.
[5] Reissner, E., 1959, "On Finite Bending of Pressurized Tubes," ASME J. Appl. Mech., **26**, pp. 386–392.
[6] Fabian, O., 1977, "Collapse of Cylindrical, Elastic Tubes Under Combined Bending, Pressure and Axial Loads," Int. J. Solids Struct., **13**(12), pp. 1257–1270.
[7] Calladine, C. R., 1983, *Theory of Shell Structures*, Cambridge University, Cambridge, UK, Chap. 16.
[8] Tatting, B. F., and Gurdal, Z., 1997, "The Brazier Effect for Finite Length Composite Cylinders Under Bending," Int. J. Solids Struct., **34**(12), pp. 1419–1440.
[9] Li, L. Y., 1996, "Bending Instability of Composite Tubes," J. Aerosp. Eng., **9**(2), pp. 58–61.
[10] Li, L. Y., and Kettle, R., 2002, "Nonlinear Bending Response and Buckling of Ring-Stiffened Cylindrical Shells Under Pure Bending," Int. J. Solids Struct., **39**(3), pp. 765–781.
[11] Guarracino, F., 2003, "On the Analysis of Cylindrical Tubes Under Flexure: Theoretical Formulations, Experimental Data and Finite Element Analyses," Thin-Walled Struct., **41**(2–3), pp. 127–147.
[12] Firer, M., and Sheinman, I., 1995, "Nonlinear Analysis of Laminated Noncircular Cylindrical Shells," Int. J. Solids Struct., **32**(10), pp. 1405–1416.
[13] Hutchinson, J. W., 1968, "Buckling and Initial Postbuckling Behavior of Oval Cylindrical Shells Under Axial Compression," ASME J. Appl. Mech., **35**(1), pp. 66–72.
[14] Zheleznov, L. P., and Kabanov, V. V., 2002, "Nonlinear Deformation and Stability of Noncircular Cylindrical Shells Under Internal Pressure and Axial Compression," ASME J. Appl. Mech. Tech. Phys., **43**(4), pp. 617–621.
[15] Volpe, V., Chen, Y. N., and Kempner, J., 1980, "Buckling of Orthogonally Stiffened Finite Oval Cylindrical Shells Under Axial Compression," AIAA J., **18**(5), pp. 571–580.
[16] Tang, S. C., Chu, C. C., and Yeung, K. S., 1985, "Collapse of Long, Noncircular, Cylindrical Shells Under Pure Bending," Comput. Struct., **21**(6), pp. 1345–1353.
[17] Corona, E., and Kyriakuxs, S., 1988, "On the Collapse of Inelastic Tubes Under Combined Bending and Pressure," Int. J. Solids Struct., **24**(5), pp. 505–535.
[18] Brush, D. O., and Almroth, B. O., 1975, *Buckling of Bars, Plates and Shells*, Int. Student ed., McGraw-Hill Kogakusha, Ltd., Tokyo, Japan, Chap. 5.
[19] Simitses, G. J., 1986, *An Introduction to the Elastic Stability of Structures*, Reprint ed., Krieger, Malabar, FL, Chap. 1.
[20] Ventsel, E., and Krauthammer, T., 2001, *Thin Plates and Shells: Theory, Analysis, and Applications*, Marcel Dekker, Inc., New York.
[21] Houliara, S., and Karamanos, S. A., 2006, "Buckling and Post-Buckling of Long Pressurized Elastic Thin-Walled Tubes Under In-Plane Bending," Int. J. Non-Linear Mech., **41**(4), pp. 491–511.